Evaluation of Convolutional Neural Network Architectures for Stress Detection in *Eucalyptus saligna* Using Multispectral UAV Imagery

Sally Déborah Pereira da Silva[1]; Lúcio de Paula Amaral[2]; Roberta Aparecida Fantinel[3], Vinicius Richter[4], Norton Borges Junior[5]

[1]Engenheira Florestal, Pós-graduanda (Doutorado em Engenharia Florestal) - PPGEF/UFSM, UFSM, Santa Maria-RS, Brasil; sallydeborah@outlook.com +55 (91) 98595-1775
[2]Engenheiro Florestal, Professor - DER-CCR/UFSM; PPGAP e PPGEF, UFSM, Santa Maria -RS, Brasil; lucio.amaral@ufsm.br
[3]Engenheira Florestal, Pós-doutoranda-Departamento de Ciências Florestais e da Madeira, Universidade Federal do Espírito Santo (UFES)
[4]Computer Science Student, Instituto Federal Farroupilha, Frederico Westphalen, RS, Brazil. E-mail: vinicius00rich@gmail.com
[5] Pesquisador da empresa florestal CMPC Brasil, Guaíba-RS, PPGEF/UFSM, UFSM, e-mail: norton.borges@cmpcrs.com.br

17th International Conference on Precision Agriculture and 11th Brazilian Congress on Precision and Digital Agriculture

13-15 July 2026

Porto Alegre, Brazil

Abstract.
Root malformation disorder (RMD) is a significant abiotic condition that impairs water and nutrient uptake in *Eucalyptus saligna*, leading to physiological stress and reduced stand uniformity. Early detection in commercial plantations is hampered by the extensive spatial scale and logistical limitations of manual field inspections. In this context, the present study evaluated the performance of three convolutional neural network (CNN) architectures, U-Net, U-Net++, and Attention U-Net, in detecting RMD symptoms in a six-month-old clonal *E. saligna* stand. Multispectral data were acquired with a MicaSense RedEdge-MX sensor (five bands). Three vegetation indices (VIs), Normalized Difference Red Edge (NDRE), Canopy Chlorophyll Content Index (CCCI), and Plant Senescence Reflectance Index (PSRI), were used as model inputs. The classification scheme comprised four distinct classes: (0) Healthy plants, (1) Diseased plants (with RMD symptoms), (2) Dead plants, and (3) Soil/residue. A labeled dataset containing 1,262 polygons across these plant classes was split into 70% for training and 30% for CNN model validation. The results indicated that the CCCI index consistently outperformed NDRE and PSRI across all architectures. Attention U-Net achieved the highest F1 score for plants with RMD symptoms (83.87%), with 92.86% accuracy and 76.47% recall. However, the standard U-Net demonstrated superior sensitivity for early detection, achieving 82.35% recall with minimal confusion between healthy and diseased plant classes. Overall accuracy exceeded 94% for all three configurations. This study demonstrates that integrating multispectral images obtained through RPAS with CNN architecture allows for the detection of RMD, providing a robust tool for precision forestry and targeted management interventions.

Keywords. *Abiotic stress; Vegetation indices; Root diseases; Precision forestry*

1 Introduction

Brazilian silviculture constitutes one of the principal segments of the national agribusiness sector, with particular emphasis on *Eucalyptus* spp. stands, which support strategic production chains such as pulp and paper, charcoal-based steelmaking, and solid wood products (IBÁ, 2025). In addition to its economic relevance, the forest sector plays a socio-environmental role by contributing to job creation, regional development, and the reduction of pressure on native vegetation remnants through the supply of raw materials produced in planted areas.

In the context of pulp and paper production, especially in southern Brazil, the species *Eucalyptus saligna* Smith (*E. saligna*), belonging to the botanical family Myrtaceae, is widely used in commercial plantations due to its high productivity, rapid growth, adaptability to diverse environmental conditions, and tolerance to frost (Kikuti and Namikawa, 1990). In *Rio Grande do Sul*, where cultivation is extensive, biotic and abiotic stresses are recurrent and may compromise early development and stand uniformity. Although *E. saligna* exhibits edaphic plasticity, natural soil fertility often does not meet the nutritional demands of the crop, requiring fertilization at different stages of the production cycle (Pulito et al., 2015). The efficiency of water and nutrient uptake depends directly on the integrity of the root system, whose functionality regulates plant growth and physiological balance; thus, root alterations may trigger anatomical, physiological, and morphological responses, ultimately affecting canopy vigor (Abreu et al., 2022).

In this scenario, commercial *E. saligna* plantations in southern Brazil may exhibit root malformation disorder (RMD), an abiotic disorder that limits water and nutrient absorption to levels compatible with plant demand, resulting in symptoms consistent with water and/or nutritional deficiency and an imbalance between root and shoot systems. RMD is frequently associated with deformation of the root system during the nursery phase or at planting, as well as with soil compaction and/or waterlogging conditions (Alfenas et al., 2004). Field monitoring is feasible; however, it presents operational limitations at large scales due to cost, time constraints, and the need for systematic inspections conducted by trained and specialized labor, which is increasingly scarce in forest companies. In this context, remote sensing (RS) using Remotely Piloted Aircraft Systems (RPAS) represents a scalable alternative for monitoring the health of planted forests, with potential to enhance efficiency in identifying critical areas and to support silvicultural and forest management decisions (Eugenio et al., 2021; Silva et al., 2024).

Concurrently, advances in artificial intelligence (AI), particularly deep learning (DL), have expanded the possibilities for RS image analysis by reducing reliance on manual feature extraction, which is typical of traditional machine learning approaches. Among the most widely used architectures, convolutional neural networks (CNNs) designed for segmentation tasks, such as U-Net (Ronneberger et al., 2015) and its variants, stand out for their ability to model complex spatial patterns and to discriminate subtle responses associated with biotic and abiotic stresses.

In light of the above, this study aimed to evaluate the performance of three CNN architectures (U-Net, U-Net++, and Attention U-Net) in the classification and detection of different health levels of *E. saligna* in a commercial stand, with the objective of comparing the discriminative capacity of the models and discussing their applicability for monitoring at the scale of commercial forest plantations.

2 Materials and methods

2.1 Study Area

The study area corresponds to a commercial Eucalyptus saligna stand owned by CMPC Brasil, located in the rural area of the municipality of São Gabriel, within the physiographic region of Campanha Gaúcha, in the western border of the state of Rio Grande do Sul, Brazil. The plantation is part of the Vacacaí Project (Figure 1) and is currently under a production rotation cycle. In the present cycle, the stand was replanted with clonal *E. saligna* seedlings and, at the time of data acquisition, was six months old, with a spacing of 3.5 × 2.14 m.

The regional climate is classified as humid subtropical (Cfa), with a mean annual temperature above 18 °C and an average annual precipitation of approximately 1,650 mm (Alvares et al., 2013). The predominant soils in the floodplains are Haplic Eutrophic Planosols with sandy characteristics. At higher elevations, Red Dystrophic Arenic Ultisols and Orthic Quartzarenic Entisols occur, both with sandy texture and high susceptibility to erosion (Embrapa, 2025).

Fig 1. Location of the experimental area within the clonal *Eucalyptus saligna* plantation, Vacacaí Project/CMPC, São Gabriel, Rio Grande do Sul, Brazil.

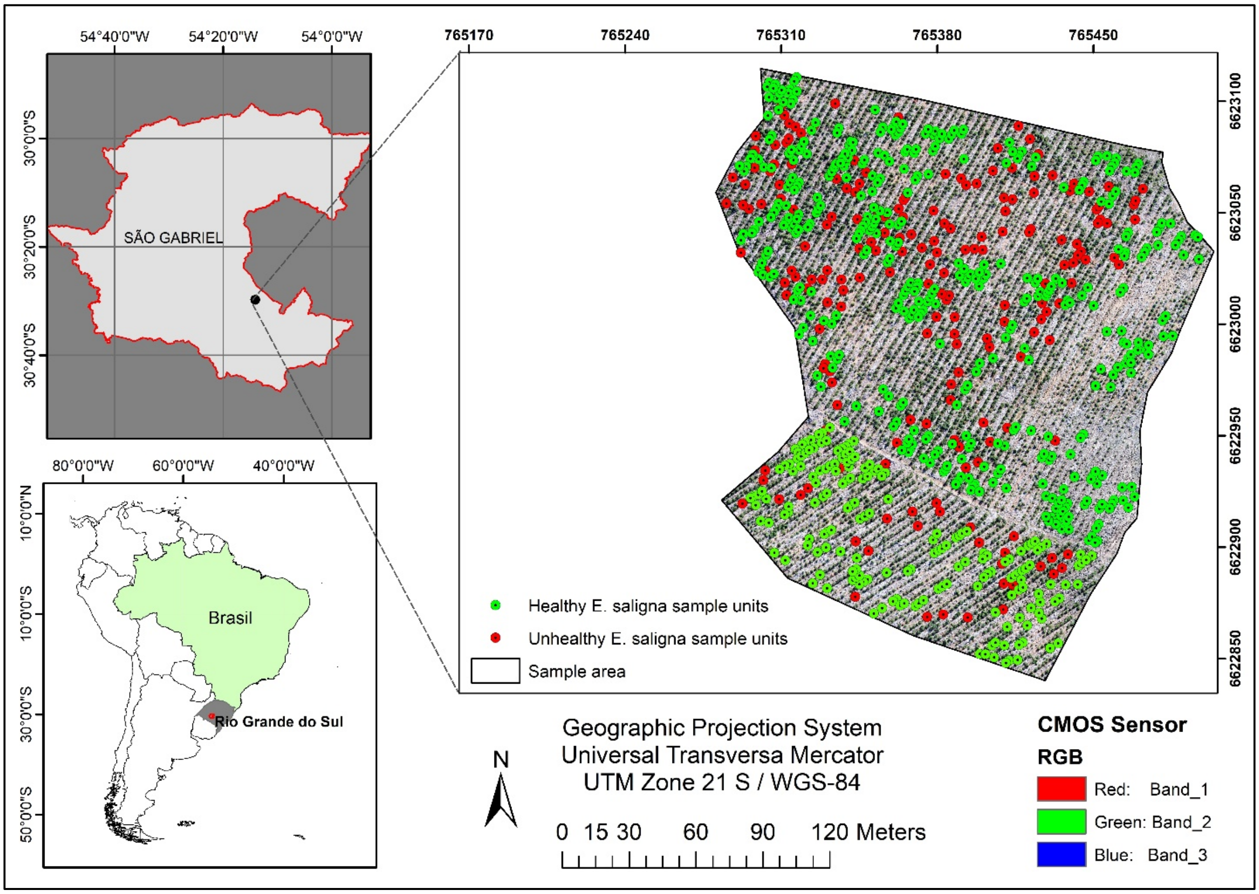

2.2 Field data acquisition and sampling

For field sampling, 15 *E. saligna* plants were randomly selected for each health class, totaling 30 individuals. The classes were defined according to the following criteria:

(i) Healthy plants: individuals with green leaves, vigorous and uniform growth, straight stems, absence of visible deformities, and a well-developed root system.

(ii) Unhealthy plants (symptomatic of RMD): individuals exhibiting reddish-brown leaves (bronzing appearance), reduced canopy density, decreased growth, collar thickening, susceptibility to lodging or stem breakage, and a root system presenting deformities.

Subsequently, a four-hectare sampling area was delineated, within which representative sampling units of the two health classes were defined. The selection of these units was based on direct image interpretation and on-site inspection of plant morphological characteristics. All sampled plants were georeferenced, enabling subsequent data extraction from vegetation index mosaics and ensuring consistent characterization of the health classes adopted as reference.

2.2 Spectral data acquisition

Multispectral images were acquired on April 30, 2025, under direct solar illumination and cloudless sky conditions, using a MicaSense RedEdge-MX® camera (MicaSense Inc., Seattle, WA, USA). The sensor captures five narrow spectral bands: B1 (blue, 475 ± 40 nm), B2 (green, 560 ± 20 nm), B3 (red, 668 ± 20 nm), B4 (red-edge, 717 ± 10 nm), and B5 (near-infrared – NIR, 840 ± 40 nm). The system includes a Downwelling Light Sensor (DLS2), mounted on the RPAS and connected to the camera, responsible for recording incident irradiance, geographic coordinates, and sensor orientation, information used for radiometric correction and image orthorectification. Radiometric calibration was performed based on albedo values obtained from a calibration panel provided by the manufacturer.

The camera was mounted on a Phantom 4 Advanced Plus® multirotor RPAS (Shenzhen DJI Sciences and Technologies, Shenzhen, China), equipped with a 20-megapixel CMOS sensor for RGB image acquisition, a mechanical shutter, and an approximate flight endurance of 30 minutes. Flight planning and execution followed a standardized protocol, including flight plan definition, placement of ground control points (GCPs), system operational checks, and takeoff and landing procedures, in order to ensure the geometric and radiometric quality of the data.

The flight plan was designed using the Precision Flight application (v. 2.4.2), with an altitude of 60 m above ground level, resulting in a ground sampling distance (GSD) of approximately 4.18 cm per pixel, flight speed of 10 m s^{-1}, 75% forward overlap, and 70% side overlap. Image acquisition was conducted between 10:00 and 11:00 a.m. (UTC−3).

To support georeferencing, GCPs were uniformly distributed across the stand and positioned in easily visible locations. The coordinates of the central point of each GCP were obtained using GNSS with the Precise Point Positioning (PPP) method. For post-processing, the data were exported in RINEX format and submitted to the IBGE-PPP service, ensuring greater positional consistency for the derived products.

2.3 Photogrammetric processing and product generation

Photogrammetric processing was performed using Agisoft Metashape® software (v. 2.2.1, Agisoft LLC, St. Petersburg, Russia). Radiometric correction was applied based on irradiance data recorded by the DLS2 sensor and albedo values obtained from the calibration panel, in order to standardize reflectance values across images and spectral bands. The processing workflow included: (i) image alignment, (ii) point cloud generation, (iii) digital surface model construction, and (iv) production of band-specific multispectral orthomosaics. The orthomosaics were exported with a spatial resolution of 4.18 cm per pixel, in the UTM coordinate system, zone 21S, datum WGS-84.

From these products, three vegetation indices (VIs) were selected based on the study by da Silva et al. (2026), considering the available spectral bands and their association with physiological stress and canopy cover. The VIs were calculated from the multispectral orthomosaics clipped to the sampling area, using the stand boundary shapefile as a spatial mask. Processing was conducted in an automated manner within the R environment, using the *terra* (Hijmans et al., 2022) and *sf* (Pebesma, 2018) packages. The NDRE (Normalized Difference Red Edge Index), PSRI (Plant Senescence Reflectance Index), and CCCI (Canopy Chlorophyll Content Index) were exported in GeoTIFF format and used in subsequent analyses. A detailed description of the spectral bands employed and the mathematical equations adopted is presented in Table 1.

Table 1. Vegetation indices used for the detection of root malformation disorder in a commercial *Eucalyptus saligna* plantation.

Vegetation Indices	Equations	Reference

NDRE	$\frac{R_{NIR} - R_{REDEDGE}}{R_{NIR} + R_{REDEDGE}}$	Barnes *et al*. (2000)
CCCI	$\frac{R_{NIR} - R_{REDEDGE}/R_{NIR} + R_{REDEDGE}}{R_{NIR} - R_{RED}/R_{NIR} + R_{RED}}$	Barnes *et al*. (2000)
PSRI	$\frac{R_{RED} - R_{GREEN}}{R_{REDEDGE}}$	Merzlyak *et al*. (1999).

2.4 Dataset preparation and labeling

Based on the preliminary analysis of the experimental area, four classes of interest were defined for supervised classification: healthy plants (class 0), plants with RMD symptoms (class 1), dead plants (class 2), and soil/residues (class 3). Labeling was performed by digitizing a shapefile containing georeferenced polygons representing homogeneous and spectrally distinct areas directly onto the multispectral orthomosaic. The RGB mosaic was used as a visual reference to aid in interpretation, ensuring spatial correspondence with the field targets (values collected in the canopy projection area).

The resulting sample set comprised 594 polygons for class 0, 194 for class 1, 74 for class 2, and 400 for class 3, constituting the reference dataset used for training and evaluating the supervised models.

From the labeled polygons, image patches were extracted to construct the input dataset for the CNN models. Each sample consisted of a multichannel patch derived from the IR layers, preserving the spatial and spectral characteristics of each class. The dataset was divided into training and validation subsets, using a stratified approach to preserve class proportions, with 70% of the samples used for training and 30%.

2.5 Evaluated architectures and training configuration

Supervised classification was performed using three CNN architectures: U-Net, U-Net++ (Nested U-Net), and Attention U-Net, implemented under the same experimental configuration to enable direct performance comparison. In this study, the models were applied using a patch-based classification approach, in which each sample corresponded to a multichannel patch extracted from the spectral products. The network estimated the probability of each sample belonging to a given class, with the final output obtained through flattening, followed by a dense layer (64 neurons, ReLU activation) and a softmax layer.

The models were configured to process inputs in the format N × N × C, where N represents the spatial context size and C the number of spectral bands and/or derived variables used as predictors. In all architectures, the encoder consisted of successive convolutional blocks and max-pooling operations, whereas the decoder employed upsampling and feature map concatenation through skip connections. In the Attention U-Net architecture, attention mechanisms were incorporated into the skip connections to modulate the contribution of encoder features during the reconstruction stage.

Fig 2. Schematic representation of the U-Net, U-Net++, and Attention U-Net architectures used for multiclass classification for the detection of root malformation disorder in a commercial *Eucalyptus saligna* plantation.

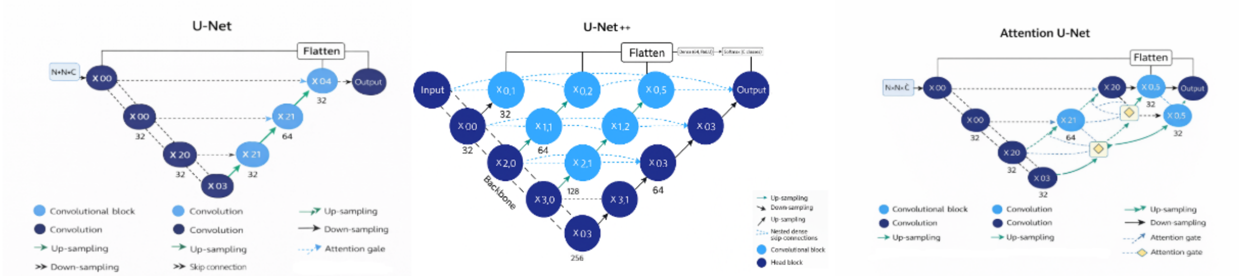

The models were trained using focal loss (γ = 1.5 α) and the Adam optimizer, with an initial learning rate of 3×10^{-4} and automatic adjustment via ReduceLROnPlateau. Convergence was monitored through minimization of validation loss (val_loss), with early stopping applied. Considering the applied objective of the study, model selection for generating the final prediction map prioritized performance on the *Unhealthy plants* class, primarily evaluated by recall and analysis of confusion matrices, in order to minimize false negatives.

From a conceptual perspective, U-Net was originally proposed for semantic segmentation in biomedical images, combining an encoder–decoder structure with skip connections to preserve spatial detail during reconstruction (Ronneberger et al., 2015). U-Net++ (Nested U-Net) extends this formulation by introducing nested dense connections between encoder and decoder, reducing the semantic gap between feature maps at different levels and promoting multiscale feature fusion (Zhou et al., 2019). Attention U-Net incorporates attention mechanisms into the skip connections, enabling the model to suppress irrelevant regions and emphasize informative areas during decoding, which may enhance discrimination of subtle patterns (Oktay et al., 2018).

All code was executed on a system running Ubuntu 24.04 Linux, equipped with a 12th Gen Intel® Core™ i5-12450H processor (Intel, Santa Clara, CA, USA) and an NVIDIA Quadro RTX 2050 GPU (16 GB) (NVIDIA, Santa Clara, CA, USA). The libraries used included: geopandas 0.14.4, rasterio 1.3.9, scikit-learn 1.3.2, tensorflow 2.13.1 with keras 2.13.1, pandas 2.0.3, matplotlib 3.7.5, and seaborn 0.12.2.

2.6 Performance evaluation and comparative analysis

Model performance was evaluated using validation datasets composed of samples not used during model training. The selected metrics aimed to assess both overall classification performance and class-specific discriminative capacity.

Accuracy provides a general measure of correctly classified instances, while precision and recall quantify the trade-off between false positives and false negatives, respectively. The F1-score summarizes this relationship as the harmonic mean of precision and recall, being particularly suitable for imbalanced datasets.

In addition, confusion matrices were analyzed to provide a detailed evaluation of classification errors and to better understand misclassification patterns among classes. Class-wise metrics were computed under a one-vs-rest (OVR) scheme, enabling the assessment of model performance for each class independently.

Precision for class c (Equation 1) is defined as the ratio between correctly predicted instances of class c and the total number of instances predicted as belonging to class c.

Recall for class c (Equation 2) is defined as the ratio between correctly predicted instances of class c and the total number of instances that truly belong to class c.

The F1-score (Equation 3) corresponds to the harmonic mean of precision and recall for a given class.

Accuracy (Equation 4) is defined as the ratio between the number of correctly classified instances and the total number of evaluated samples.

$$\text{Eq.1: } Pc = \frac{True\ Positive\ (TPc)}{TPc\ + False\ positive (FPc)} \quad (1)$$

$$\text{Eq. 2: } Rc = \frac{TPc}{TPc + False\ negative\ (FNc)} \quad (2)$$

$$\text{Eq. 3: } F1\ Score = 2 * \frac{Pc * Rc}{Pc + Rc} \quad (3)$$

$$\text{Eq. 4: Accuracy} = \frac{Number\ of\ correct\ classifications}{Total\ samples} \quad (4)$$

3 Results and discussion

Table 2 presents the performance by class for the evaluated architectures and IVs. Considering the main objective of this study, the detection of plants with symptoms of root malformation disorder (RMD), the CCCI index showed consistently superior performance to NDRE and PSRI in all models, indicating greater discriminative capacity for this condition.

In terms of balance between precision and recall, Attention U-Net combined with CCCI obtained the highest F1 score for the target class, indicating a more balanced classification performance and less tendency to false positives. However, it is important to highlight that the U-Net architecture combined with CCCI achieved higher recall values, demonstrating greater sensitivity in identifying symptomatic plants.

From an operational standpoint, this distinction is relevant because a higher recall rate is associated with a lower false negative rate, which is crucial for the early detection of stress in commercial crops.

Table 2. Performance metrics obtained for the four health classes of *Eucalyptus saligna* using the Attention U-Net, U-Net++, and U-Net architectures, with CCCI, PSRI, and NDRE vegetation indices as predictor variables. Metrics were calculated on a class-wise basis under the one-vs-rest scheme for the detection of root malformation disorder in a commercial *Eucalyptus saligna* plantation.

Class	Arquitetura	Model	Precision (%)	Recall (%)	F1-score (%)	Accuracy (%)
Healthy plants	Attention U-Net	CCCI	95.58	97.19	96.38	96.34
		PSRI	92.18	92.70	92.44	92.39
		NDRE	97.01	91.01	93.91	94.08
Unhealthy plants	Attention U-Net	CCCI	92.86	76.47	83.87	97.18
		PSRI	55.81	70.59	62.34	91.83
		NDRE	61.54	70.59	65.75	92.96
Dead plants	Attention U-Net	CCCI	36.84	58.33	45.16	95.21
		PSRI	71.43	83.33	76.92	98.31
		NDRE	25.00	25.00	25.00	94.93
Soil/ residue	Attention U-Net	CCCI	97.64	94.66	96.12	97.18
		PSRI	100.00	95.42	97.66	98.31
		NDRE	93.23	94.66	93.94	95.49
Class	**Arquitetura**	**Model**	**Precision (%)**	**Recall (%)**	**F1-score (%)**	**Accuracy (%)**
Healthy plants	U-Net++	CCCI	95.88	91.57	93.68	93.80
		PSRI	94.08	89.33	91.64	91.83
		NDRE	97.48	87.08	91.99	92.39
Unhealthy plants	U-Net++	CCCI	81.82	79.41	80.60	96.34
		PSRI	55.81	70.59	62.34	91.83
		NDRE	47.92	67.65	56.10	89.86
Dead plants	U-Net++	CCCI	36.00	75.00	48.65	94.65
		PSRI	100.00	58.33	73.68	98.59
		NDRE	25.00	25.00	25.00	94.93
Soil/ residue	U-Net++	CCCI	98.43	95.42	96.90	97.75
		PSRI	95.59	99.24	97.38	98.03

		NDRE	91.91	95.42	93.63	95.21

Class	Arquitetura	Model	Precision (%)	Recall (%)	F1-score (%)	Accuracy (%)
Healthy plants	U-Net	CCCI	95.95	93.26	94.59	94.65
		PSRI	96.25	86.52	91.12	91.55
		NDRE	94.83	92.70	93.75	93.80
Unhealthy plants	U-Net	CCCI	75.68	82.35	78.87	95.77
		PSRI	52.83	82.35	64.37	91.27
		NDRE	61.54	70.59	65.75	92.96
Dead plants	U-Net	CCCI	33.33	41.67	37.04	95.21
		PSRI	81.82	75.00	78.26	98.59
		NDRE	38.46	41.67	40.00	95.77
Soil/ residue	U-Net	CCCI	96.15	95.42	95.79	96.90
		PSRI	97.71	97.71	97.71	98.31
		NDRE	93.02	91.60	92.31	94.37

This result can be attributed to the greater sensitivity of the CCCI to variations in chlorophyll content and canopy structure, which are directly affected by root malformation disorder and associated physiological stress. In contrast, the NDRE and PSRI showed inferior and more variable performance, suggesting less sensitivity to specific spectral responses associated with DMR (da Silva et al., 2026).

The confusion matrix analysis (Figure 3) further indicates that the U-Net architecture combined with the CCCI achieved the highest sensitivity for plants with DMR symptoms, with a higher rate of correct classifications and less confusion with healthy plants. This configuration is therefore more suitable in operational contexts where minimizing false negatives is a priority.

For the other classes, performance was generally high and consistent across models. However, the dead plant class showed greater variability, indicating greater difficulty in spectral discrimination, particularly due to confusion with soil/residues in more advanced stages of degradation.

Fig 3. Percentage confusion matrices for the classification of *Eucalyptus saligna* health status in a commercial plantation using the Attention U-Net, U-Net++, and U-Net architectures with the CCCI index.

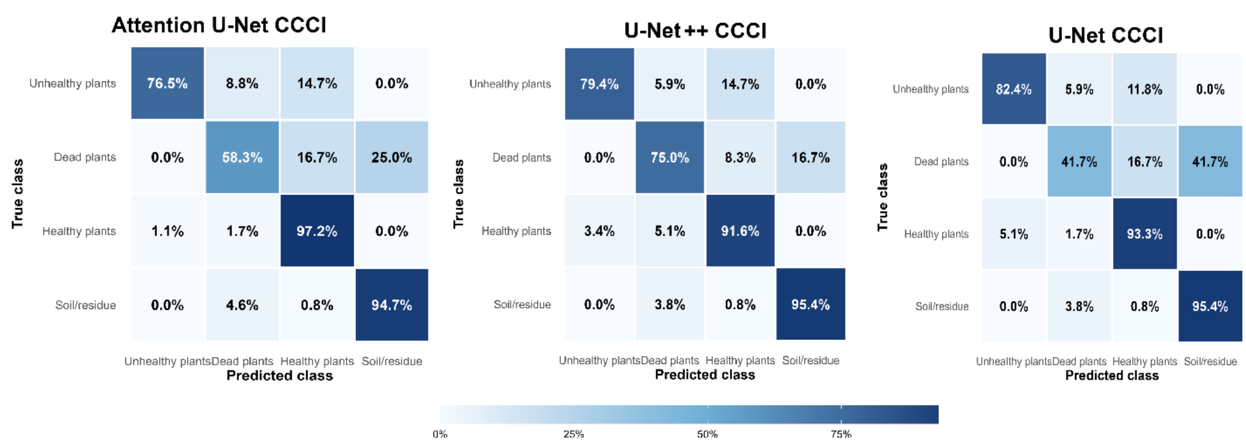

For semantic segmentation of canopies and vegetation classes, architectures such as U-Net and DeepLab represent the state of the art, achieving accuracies above 90% in different scenarios (Zhao et al., 2023). However, in a study focused on species classification based on canopy data, a task more complex than that addressed herein, performance ranged from 40% to 92%, depending on the sensor, architecture, and adopted protocol. This finding highlights that spectral selection and target definition exert influence as significant as the network architecture itself (Huang et al., 2024).

Other architectures have also demonstrated consistent performance in forest applications. Instance segmentation approaches, such as Mask R-CNN, have been successfully applied to crown delineation and discrimination between live and dead trees in forest decline scenarios, achieving high precision and F1-score when associated with high spatial resolution imagery and robust annotations (Lucas et al., 2024). However, these methods prioritize individual object detection and do not represent diffuse physiological patterns in the canopy, such as the root stress evaluated in this study, with the same level of precision.

Recent adaptations of U-Net variants have likewise achieved high performance in multiclass forest scenarios affected by pests (Machuca & Markov, 2025; Kerchev et al., 2024). Although these studies involve different target species and symptoms, the consistency of segmentation results reinforces the suitability of U-Net–based models for detecting canopy alterations associated with root malformation disorder.

The learning curves obtained using the CCCI index (Figure 4) indicate consistent convergence between the evaluated architectures (U-Net++, U-Net, and Attention U-Net). A rapid increase in performance was observed during the initial epochs, followed by progressive stabilization, indicating stable training and gradual error reduction. In the accuracy curves (Fig. 4a), all models exhibited sharp initial gains, with convergence occurring after approximately 40 to 50 epochs. The Attention U-Net stabilized slightly earlier and maintained marginally higher accuracy values, while the U-Net and U-Net++ showed similar trends with small intermediate oscillations.

Similarly, the loss curves (Fig. 4b) showed a sharp drop during initial training, followed by gradual stabilization. Among the models evaluated, the Attention U-Net demonstrated a more efficient convergence trajectory and slightly lower final loss values, although the overall differences between the architectures were relatively small.

Fig 4. Performance curves per epoch for the U-Net++, U-Net, and Attention U-Net architectures using the CCCI index for *Eucalyptus saligna*: **(a) Evolution of accuracy throughout training epochs. (b) Evolution of the loss function during training.**

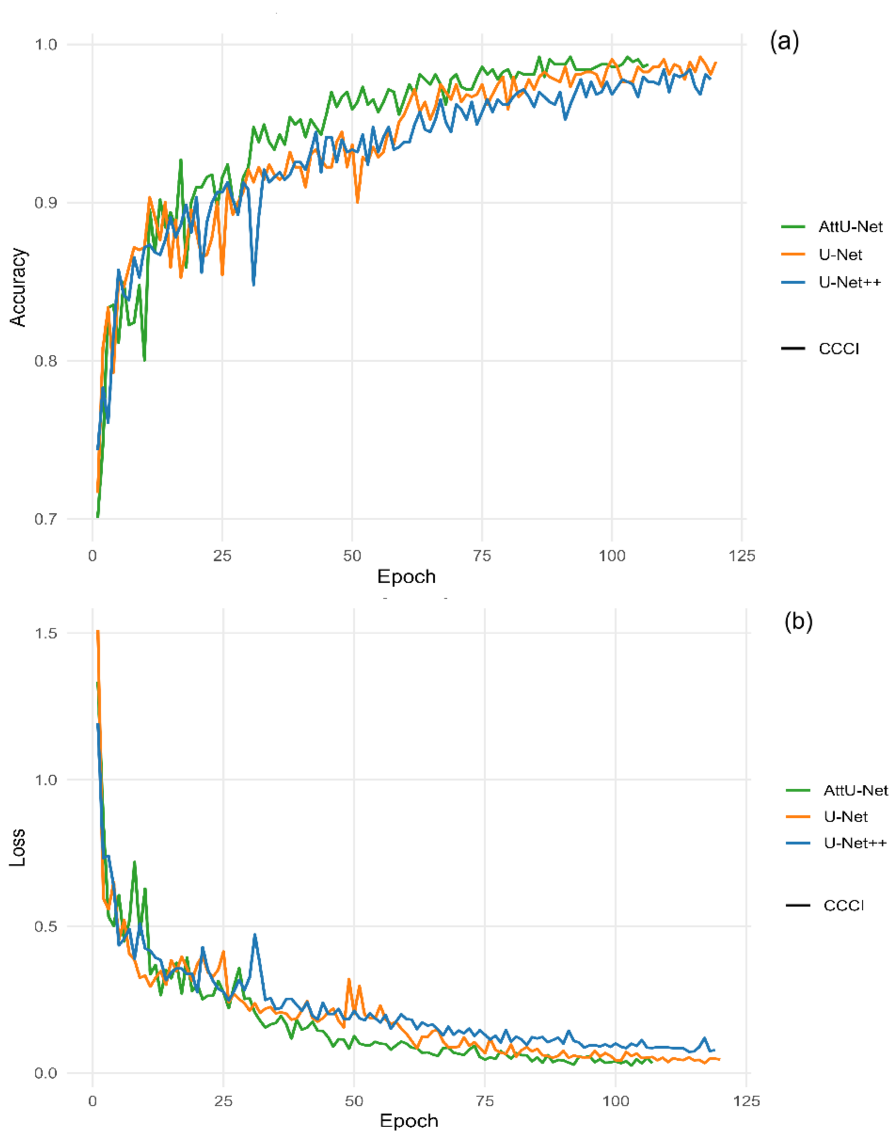

Based on the integrated analysis of evaluation metrics, confusion matrices, and learning curves, the U-Net model trained with the CCCI index was selected for application in the experimental area. This selection was primarily motivated by its greater sensitivity to the symptomatic class of RMD and less confusion with healthy plants, critical factors for the early detection of stress.

The selected model was then applied to generate the spatial distribution of *E. saligna* health classes (healthy plants, plants with RMD symptoms, and dead plants) throughout the study area (Figure 5).

Fig 5. Spatial distribution of *Eucalyptus saligna* health classes in a commercial plantation using the U-Net model based on the CCCI index. In (a), RGB image acquired by RPAS over the same area, used as visual reference. In (b), continuous CCCI index map indicating vigor gradient (red to blue). In (c), detailed crown-level classification, with class delineation: plants symptomatic of root malformation disorder (yellow), healthy plants (green), dead plants (brown), and soil/residues (gray).

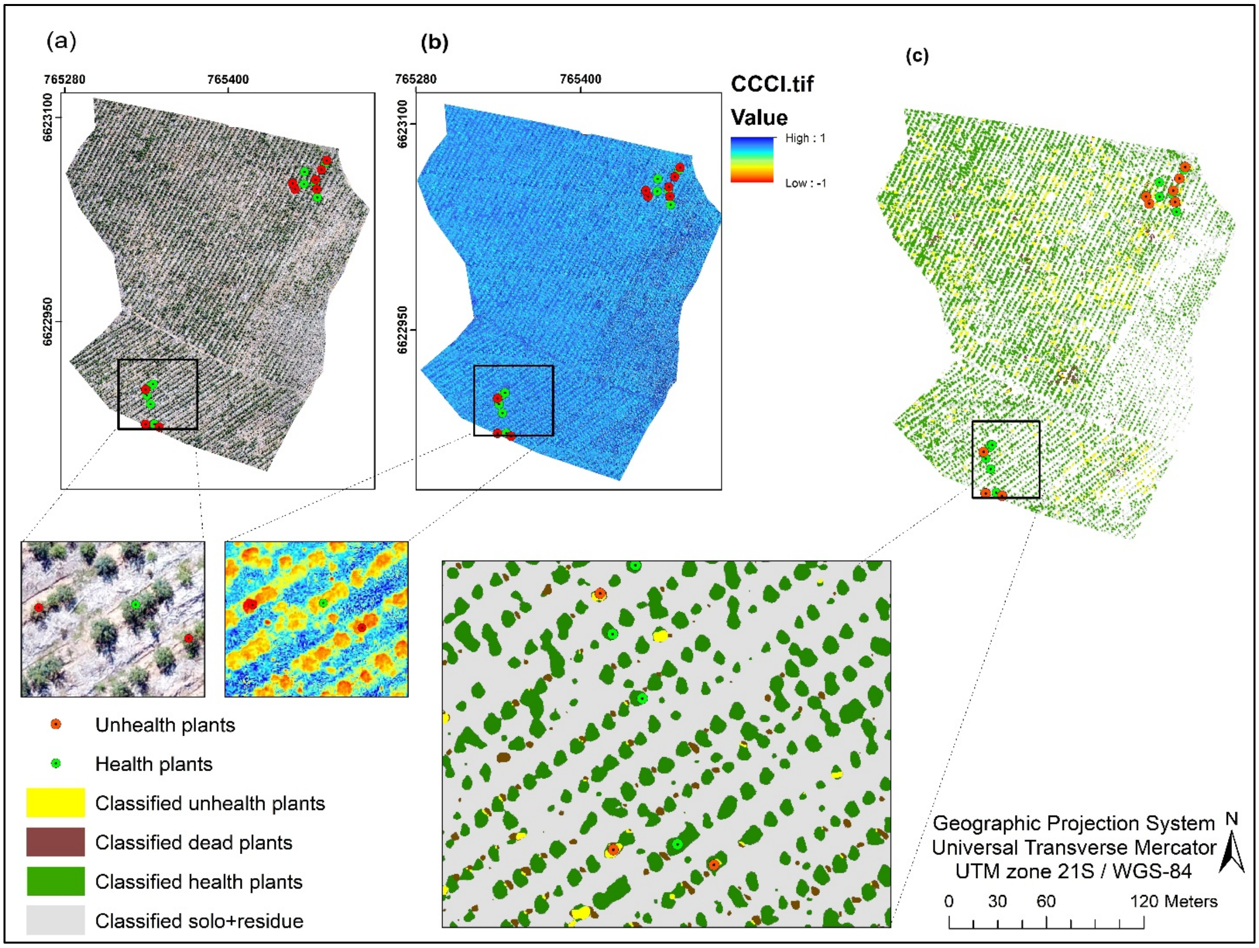

Based on the classification shapefiles, it was possible to quantify the coverage of the classes within the four-hectare plot. The area occupied by the plants corresponded to 25.9% of the plot (1.04 ha), considering only the vegetated classes. Within this area, 96.8% of the plants were classified as healthy, 2.2% as symptomatic of RMD (wood mosaic disease), and 1.0% as dead. Overall, the group of diseased plants (symptomatic of RMD + dead) represented 3.2% of the vegetated area.

It is important to note that regrowth and plants located between the rows were included in this evaluation, which may influence the final proportions of the classes when considering only the planted seedlings.

These results indicate that the proposed approach is capable of spatially detecting and quantifying stress conditions at an early stage at the plot level, allowing the identification of relatively small proportions of affected plants. From an operational perspective, this level of detail is particularly relevant for precision forestry, as it enables targeted interventions in specific areas, rather than uniform management practices across the entire plot. In this context, the performance obtained with the U-Net architecture is consistent with results reported in the literature. Ahmed et al. (2021), using images acquired by RPAS, achieved an accuracy of 0.95 in the segmentation of multiple objects, demonstrating the robustness of this architecture for high-resolution applications. Furthermore, Bragagnolo et al. (2021) applied U-Net to classify vegetated and non-vegetated areas in the Amazon, achieving an overall accuracy of 94.7%.

4 Conclusion

The present study demonstrated that the three evaluated DL-CNN architectures are effective in detecting *Eucalyptus saligna* plants affected by root malformation disorder (RMD), highlighting their potential for monitoring and supporting health management in planted forests.

Among the vegetation indices analyzed, CCCI exhibited greater consistency and discriminative capacity for the target class (RMD-symptomatic plants), achieving a better balance between precision and recall across architectures. Attention U-Net achieved the highest F1-score for the target class, whereas U-Net demonstrated greater sensitivity, with lower confusion between symptomatic and healthy plants, an important aspect when the operational priority is minimizing false negatives.

Overall, the results indicate that the integration of RGB and multispectral imagery acquired by RPAS, vegetation indices sensitive to physiological vigor, and U-Net–based architectures constitutes a robust approach for forest health assessment at the commercial stand scale for *Eucalyptus saligna* in southern Brazil. The proposed methodology enables early identification of canopy alterations associated with root malformation, providing technical support for more precise and targeted management interventions.

Acknowledgments

This study was supported by the Coordenação de Aperfeiçoamento de Pessoal de Nível Superior (CAPES; Finance Code 001), the Graduate Program in Forest Engineering (PPGEF) at the Federal University of Santa Maria (UFSM), and Research Project No. 060220 (GAP-CCR/UFSM). The authors also acknowledge CMPC Brasil for granting access to the study area and the Aquarius Project at UFSM for providing the multispectral sensor (MicaSense RedEdge-MX).

References

Abreu, M. C., Soares, A. A. V., de Freitas, C. H., & Martins, F. B. (2022). Transpiration and growth responses by Eucalyptus species to progressive soil drying. *Journal of Forestry Research*, *33*(5), 1529-1543. https://doi.org/10.1007/s11676-021-01448-z

Ahmed, I., Ahmad, M., & Jeon, G. (2021). A real-time efficient object segmentation system based on U-Net using aerial drone images. *Journal of Real-Time Image Processing*, *18*(5), 1745-1758.

Alfenas, A. C., Zauza, E. A. V., Mafia, R. G., & Assis, T. F. (2004). Clonagem e doenças do eucalipto, Viçosa MG. *Universidade Federal de Viçosa. Universidade Federal de Viçosa*.

Alvares, C. A., Stape, J. L., Sentelhas, P. C., Gonçalves, J. D. M., & Sparovek, G. (2013). Köppen's climate classification map for Brazil. *Meteorologische zeitschrift*, *22*(6), 711-728. https://doi.org/10.1127/0941-2948/2013/0507.

Barnes, E. M., Clarke, T. R., Richards, S. E., Colaizzi, P. D., Haberland, J. U. L. I. O., Kostrzewski, M., ... & Moran, M. S. (2000, July). Coincident detection of crop water stress, nitrogen status and canopy density using ground based multispectral data. In *Proceedings of the fifth international conference on precision agriculture, Bloomington, MN, USA* (Vol. 1619, No. 6).

Bragagnolo, L., da Silva, R. V., Grzybowski, J. M. V. (2021). Amazon Forest cover change mapping based on semantic segmentation by U-nets. Ecol. Inf. 62, 12. doi: 10.1016/j.ecoinf.2021.101279

da Silva, S. D. P., Richter, V., Junior, N. B., Ferreira, R. A., Ferreira, G. V., Amado, T. J. C., ... & de Paula Amaral, L. (2026). Remote detection of root malformation disorder in Eucalyptus saligna using UAV multispectral imagery and U-Net++. *Computers and Electronics in Agriculture*, *244*, 111522.

Embrapa. Centro Nacional de Pesquisa de Solos. *Sistema Brasileiro de Classificação de Solos*. Brasília: Embrapa -SPI; Rio de Janeiro: Embrapa Solos, 2025. 6ª ed. 355p.

Eugenio, F. C., Badin, T. L., Fernandes, P., Mallmann, C. L., Schons, C., Schuh, M. S., ... & Pereira da Silva, S. D. (2021). Remotely Piloted Aircraft Systems (RPAS) and machine learning: A review in the context of forest science. *International Journal of Remote Sensing*, *42*(21), 8207-8235. 10.1080/01431161.2021.1975845

Hijmans, R. J., Bivand, R., Forner, K., Ooms, J., Pebesma, E., & Sumner, M. D. (2022). Package 'terra'. *Maintainer: Vienna, Austria*, *384*. Available at: https://cran.r-project.org/web/packages/terra/index.html

Huang, Y., Ou, B., Meng, K., Yang, B., Carpenter, J., Jung, J., & Fei, S. (2024). Tree species classification from UAV canopy images with deep learning models. *Remote Sensing*, *16*(20), 3836. https://doi.org/10.3390/rs16203836

IBÁ. 2025. Relatório 2025. São Paulo. Available from: https://iba.org/wp-content/uploads/2025/05/relatorio2024.pdf [accessed 03 september 2025].

Kerchev, I. A., Markov, N. G., Machuca, C. R., & Tokareva, O. S. (2024). Classification of pest-damaged coniferous trees in unmanned aerial vehicles images using convolutional neural network models. *Computer research and modeling*, *16*(5), 1271-1294. https://doi.org/10.20537/2076-7633-2024-16-5-1271-1294

Kikuti, P., & Namikawa, I. S. (1990). Estudo da interação clone x níveis da adubação em Eucalyptus saligna. *O Papel, São Paulo*, *31*(3), 37-44.

Lee, H., Lee, C., Woo, H., & Choi, S. E. (2025). Optimal Training Sample Sizes for U-Net-Based Tree Species Classification with Sentinel-2 Imagery. *Forests*, *16*(11), 1718.

Lucas, M., Pukrop, M., Beckschäfer, P., & Waske, B. (2024). Individual tree detection and crown delineation in the Harz National Park from 2009 to 2022 using mask R–CNN and aerial imagery. *ISPRS Open Journal of Photogrammetry and Remote Sensing*, *13*, 100071. https://doi.org/10.1016/j.ophoto.2024.100071

Machuca, C. R., & Markov, N. G. (2025). Advanced neural network models for UAV-based image analysis in remote pathology monitoring of coniferous forests. *Computer Research and Modeling 17*(4), 641-663.https://doi.org/10.20537/2076-7633-2025-17-4-641-663

Merzlyak, M. N., Gitelson, A. A., Chivkunova, O. B., & Rakitin, V. Y. (1999). Non-destructive optical detection of pigment changes during leaf senescence and fruit ripening. *Physiologia plantarum*, *106*(1), 135-141. https://doi.org/10.1034/j.1399-3054.1999.106119.x

Oktay, O., Schlemper, J., Folgoc, L. L., Lee, M., Heinrich, M., Misawa, K., ... & Rueckert, D. (2018). Attention u-net: Learning where to look for the pancreas. *arXiv preprint arXiv:1804.03999*.

Pebesma, E. (2018). Simple features for R: standardized support for spatial vector data. Available at: https://cran.r-project.org/web/packages/sf/index.html

Pulito, A.P., Gonçalves, J.L., de, M., Smethurst, P.J., Alvares, C.A., Rocha, J.H.T., et al., 2015. Available nitrogen and responses to nitrogen fertilizer in Brazilian Eucalypt plantations on soils of contrasting texture. Forests, **6**: 973–991. doi:10.3390/f6040973.

Ronneberger, O., Fischer, P., & Brox, T. (2015). *U-Net: Convolutional Networks for Biomedical Image Segmentation*.

Silva, S. D. P., de Paula Amaral, L., Aparecida Fantinel, R., & Coelho Eugenio, F. (2024). RPAS-Based forest plantation health monitoring: an overview of recent progress. *International Journal of Remote Sensing*, *45*(24), 9131-9161.

Zhao, H., Morgenroth, J., Pearse, G. *et al.* A Systematic Review of Individual Tree Crown Detection and Delineation with Convolutional Neural Networks (CNN). *Curr Forestry Rep* **9**, 149–170 (2023). https://doi.org/10.1007/s40725-023-00184-3

Zhou, Z., Siddiquee, M. M. R., Tajbakhsh, N., & Liang, J. (2019). *UNet++: A Nested U-Net Architecture for Medical Image Segmentation*.